

# MixerGAN: An MLP-Based Architecture for Unpaired Image-to-Image Translation

George Cazenavette  
Robotics Institute  
Carnegie Mellon University  
gcazenav@cs.cmu.edu

Manuel Ladron De Guevara  
School of Architecture  
Carnegie Mellon University  
manuelr@andrew.cmu.edu

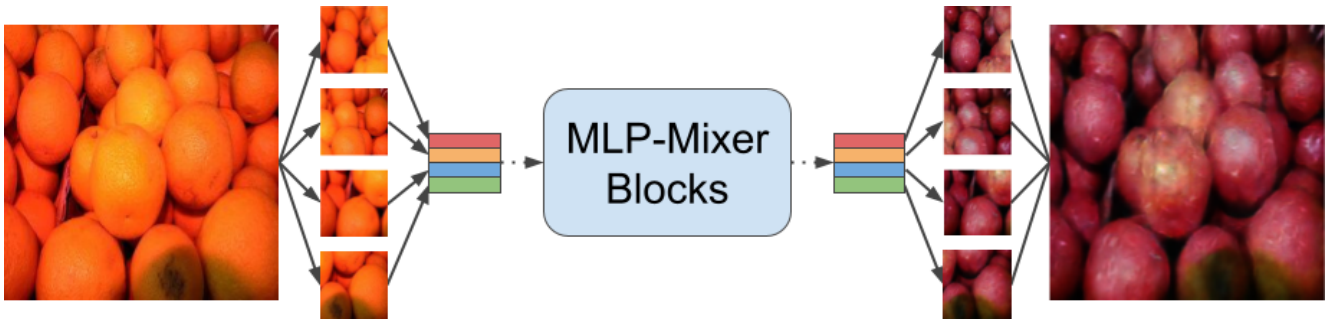


Figure 1: Overview of MixerGAN. Our generator linearly projects image patches into vectors before translating via mixer blocks and up-projecting to transfigured patches.

## Abstract

While attention-based transformer networks achieve unparalleled success in nearly all language tasks, the large number of tokens (pixels) found in images coupled with the quadratic activation memory usage makes them prohibitive for problems in computer vision. As such, while language-to-language translation has been revolutionized by the transformer model, convolutional networks remain the de facto solution for image-to-image translation. The recently proposed MLP-Mixer architecture alleviates some of the computational issues associated with attention-based networks while still retaining the long-range connections that make transformer models desirable. Leveraging this memory-efficient alternative to self-attention, we propose a new exploratory model in unpaired image-to-image translation called MixerGAN: a simpler MLP-based architecture that considers long-distance relationships between pixels without the need for expensive attention mechanisms. Quantitative and qualitative analysis shows that MixerGAN achieves competitive results when compared to prior convolutional-based methods.

## 1. Introduction

As with most visual tasks in the deep learning age, image-to-image translation has been dominated by fully convolutional neural networks since its inception [9, 28, 18]. However, the recently proposed MLP-Mixer [23] architecture showed that simple multi-layered perceptrons are still useful for visual learning in deep neural networks. While the original MLP-Mixer paper only addressed *discriminative* tasks, we propose adapting this new architecture for *generative* tasks. Since the MLP-Mixer closely resembles the transformer model originally used for sequence-to-sequence translation in natural language processing [24], we choose to evaluate the MLP-Mixer’s capabilities on image-to-image translation through our new model: MixerGAN.

Transformer models are desirable for sequence-to-sequence translation because their self-attention mechanisms account for long-range dependencies that are overlooked by the relatively small receptive fields of convolutions. As such, self-attention has been used in image-to-image translation before [22, 1, 4]. However, the extreme memory usage of self-attention mechanisms prevents them from being used effectively on whole images, even after they have been significantly down-sampled. Motivated by a

memory-efficient alternative to self-attention mechanisms, MixerGAN offers a much cheaper alternative to transformers that still accounts for long-range dependencies within an image.

Image-to-image translation is the task of learning a mapping between a source domain and a target domain. This is useful for applications such as data augmentation [15], domain adaptation [16], colorization [3], style transfer [9], or image super-resolution [11, 26]. In an ideal setting, we have source-target paired inputs and this problem can be solved using supervised learning. This is the setting of the seminal work from Isola et al. [9] where an encoder-decoder-like network translates from one domain  $X$  to another  $Y$  and vice-versa. However, finding paired data is hard, and the lack of such datasets led to the development of unsupervised approaches like CycleGAN [28], where a cycle consistency loss ensures an invertible mapping between the two domains.

Although we show that MixerGAN achieves results competitive with prior convolutional-based generative models, our goal is not to achieve state-of-the-art results or outperform any benchmarks on image-to-image translation. Instead, we establish a new baseline that is able to provide similar results as those in [28], showing that an MLP-based architecture can be used for image synthesis tasks.

In short, our primary contribution is showing that the MLP-Mixer architecture can be adapted to effectively perform unpaired image-to-image translation while accounting for long-range dependencies at a much lower cost than a transformer model.

## 2. Related Work

Throughout the evolution of sequence-to-sequence translation, it has been shown that context-awareness is critical to high-efficacy models [20]. Traditional convolutional models limit context sharing between tokens to the width of the filter, preventing the model from learning longer-range relations between distant tokens. To that end, the natural language processing community moved on from these traditional models and adopted transformer models [24] which offer connections between all tokens in the sequence while also eliminating the inductive locality bias. In this section, we first briefly review general CNN-based image-to-image translation frameworks, followed by models that propose different reinterpretations of attention mechanisms to address longer range and better informed dependencies in pixel space.

**Image-to-image translation** GAN [5] frameworks are the natural and standard approaches to image-to-image translation tasks. For instance, Isola et al. [9] use a conditional GAN that takes a source image as input instead of the standard noise vector from original GANs to learn

a mapping from said input to a target output image. A limitation of this approach is the need to have paired images from different distributions. In an effort to alleviate this constraint, Zhu et al. [28] presented a similar but more flexible framework called CycleGAN that learns a mapping from distribution  $X$  to  $Y$  without the need for paired inputs. To ensure such "unsupervised" mapping, besides the common adversarial loss, they add a cycle consistency loss with the premise that a correctly learned inverse mapping should translate the generated image back to its original distribution. Similar to this work are DiscoGAN [10] and DualGAN [27] but with different loss functions. Some other unsupervised work assume a shared latent space between source and target domains. For instance, Liu et al. proposed unsupervised image-to-image translation (UNIT) [12] building upon coupled GANs [13] which enforce source and target generators and discriminators to share parameters in low-level layers assuming the existence of a shared latent space between two such distributions. Huang et al. extended this framework to a multi-modal setting in MUNIT [8], using two latent representations for style and content.

**Attention-based image-to-image translation.** The effectiveness of attention mechanisms on language models made researchers look for similar attention algorithms for vision tasks. However, due to the quadratic cost of the attention activations over the input sequence, which makes it undesirable for high resolution images, attention has been interpreted loosely in image-to-image translation. For instance, Tang et al. [22] generate a series of foreground, background and content masks to guide the translation process, in a slightly more complex model than previous work. Mejjati et al. [1] add two more attention networks that learn foreground and background attention maps and remove instance normalization from the discriminator. In SPA-GAN [4], the discriminator learns an attention map that is fed to the generator to help focus the most discriminative object parts, but it is not composed by different masks.

Motivated by the important role of attention mechanisms and advocating for a simpler model, we propose an efficient alternative for image-to-image translation based on weighted MLPs, which aims to alleviate the problem of ignored long-range dependencies.

## 3. MixerGAN

We show that mixer blocks offer an alternative method of performing unpaired image-to-image translation that accounts for global relations not possible with vanilla convolutional blocks and in a computationally cheaper way than transformer blocks.

Formally, our goal is to train two mixer-based generators  $G : X \rightarrow Y$  and  $F : Y \rightarrow X$  that "translate" images between two distributions. We accomplish this in the same

way as the original CycleGAN by also simultaneously training two discriminators  $D_X$  and  $D_Y$  to distinguish between real and generated images.

### 3.1. Training Objective

For a more stable optimization, we employ the LS-GAN formulation [14] such that our generators  $G$  and  $F$  are then trained to minimize

$$\mathcal{L}_G = \mathbb{E}_{x \sim X} [(D_Y(G(x)) - 1)^2] \quad (1)$$

$$\mathcal{L}_F = \mathbb{E}_{y \sim Y} [(D_X(F(y)) - 1)^2]$$

Our discriminators  $D_X$  and  $D_Y$  are then simultaneously trained to minimize

$$\begin{aligned} \mathcal{L}_{D_X} = & \mathbb{E}_{x \sim X} [(D_X(x) - 1)^2] \\ & + \mathbb{E}_{y \sim Y} [D_X(F(y))^2] \end{aligned} \quad (2)$$

$$\begin{aligned} \mathcal{L}_{D_Y} = & \mathbb{E}_{y \sim Y} [(D_Y(y) - 1)^2] \\ & + \mathbb{E}_{x \sim X} [D_Y(G(x))^2] \end{aligned}$$

In accordance with the CycleGAN [28] formulation, we also regularize the cycle consistency loss between the two generators:

$$\begin{aligned} \mathcal{L}_{cyc} = & \mathbb{E}_{x \sim X} [|F(G(x)) - x|] \\ & + \mathbb{E}_{y \sim Y} [|G(F(y)) - y|] \end{aligned} \quad (3)$$

The weighted cycle consistency loss is then added to both generator losses to encourage an invertible translation.

### 3.2. Model Architecture

For comparison’s sake, we experiment with networks of similar size to those used in the original CycleGAN paper [28]. While the mixer blocks have more parameters than the convolutional blocks, our mixer models still have the same number of non-linearities and a comparable—if not lower—dimensional latent space.

In accordance with the original CycleGAN, our mixer-based generator consists of a single-layer convolutional stem followed by two strided convolutional layers for learned down-sampling and a linear patch down-projection step. The patch down-projection step is effectively a convolution where the kernel size and stride are equal to the patch size, resulting in an output representation where each pixel is a linear projection of a disjoint patch of the input. For all our experiments, we used a patch size of 8x8 and projected each patch to a token vector of length 256. The transforming part of the MixerGAN generator then consists of 9 isotropic mixer blocks (whereas the analogous part of the CycleGAN generator has 9 residual convolutional blocks). Lastly, the transformative section is followed by a linear

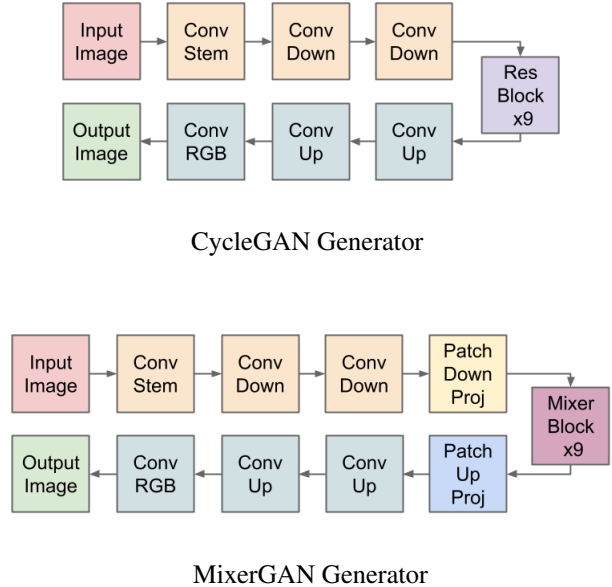


Figure 2: (Top): The CycleGAN architecture consists of 9 isotropic residual convolution blocks book-ended by down and up-sampling convolutions. (Bottom): In the MixerGAN architecture, we replace the residual blocks with MLP-Mixer blocks between down and up patch projections.

patch up-projection step, two up-sampling transposed convolutions, and a final convolution to remap the representation to the source RGB space. For our discriminator, we employ a PatchGAN in accordance with the CycleGAN paper [9].

The mixer blocks themselves directly follow the formulation given in the MLP-Mixer paper [23]. After the patch projection step, the tokens are stacked as rows such that the representation  $\mathbf{X}$  is now only two-dimensional and is of shape  $(tokens \times channels)$ . The mixer block itself consists of two Multi-Layer Perceptrons with skip connections: one for token mixing and one for channel mixing. The token-mixing MLP acts on the *columns* of the representation while the the channel-mixing MLP acts on its *rows*. If we do not expand the hidden dimension of the MLPs, then the shape of our token-mixing weights  $\mathbf{W}_1$  and  $\mathbf{W}_2$  is  $(tokens \times tokens)$ . Likewise, the shape of our channel-mixing weights  $\mathbf{W}_3$  and  $\mathbf{W}_4$  is  $(channels \times channels)$ .

Formally, the MLP-mixer block on  $\mathbf{X} \rightarrow \mathbf{Y}$  can be described by the following equations:

$$\begin{aligned} \mathbf{U} &= \mathbf{X} + \mathbf{W}_2 \text{GELU}(\mathbf{W}_1 \text{LayerNorm}(\mathbf{X})) \\ \mathbf{Y} &= (\mathbf{U}^T + \mathbf{W}_4 \text{GELU}(\mathbf{W}_3 \text{LayerNorm}(\mathbf{U})^T))^T \end{aligned} \quad (4)$$

where GELU is the Gaussian Error Linear Unit [6]. Note that our mixer blocks are isotropic such that the shape of the output is the same as the input:  $(tokens \times channels)$ . Each linear operator of the token-mixing MLP mixes as-

Activation Memory Usage Per Sample (Floats)			
#tokens	#channels	SA	TM
16x16	128	98.3k	32.8k
16x16	512	196.6k	131.1k
32x32	128	1179.6k	131.1k
32x32	512	1572.9k	524.3k
64x64	128	17301.5k	524.3k
64x64	512	18874.4k	2097.2k

Table 1: Self-attention (SA) memory usage scales linearly with channels but quadratically with tokens while token-mixing (TM) memory only scales linearly with both channels and tokens. Self-attention memory usage additionally scales linearly with the number of heads (values in table for 1-headed self-attention).

Trainable Parameters			
#tokens	#channels	SA	TM
16x16	128	49.1k	65.5k
16x16	512	786.4k	65.5k
32x32	128	49.1k	1048.6k
32x32	512	786.4k	1048.6k
64x64	128	49.1k	16777.2k
64x64	512	786.4k	16777.2k

Table 2: Self-attention’s (SA) parameter count scales quadratically strictly with channels while token-mixing’s (TM) scales quadratically strictly with tokens. However, parameter count is static and does not scale with batch size, so we don’t see the same issues as when scaling self-attention to higher batch sizes.

signs each output token as a linear combination of *all* input tokens where the linear weights depend on the token’s location. As such, the MLP-mixer, by definition, applies long-range interactions between pixels.

An overview of our MixerGAN generator and a comparison to that of CycleGAN can be found in Figure 2. Pytorch [19] implementations of our MixerGAN generator and the MLP-Mixer block itself can be found in Appendix A.

### 3.3. Computational Advantages

For this analysis, we consider all layers to be “isotropic” such that their inputs and outputs are of the same shape.

As noted in the seminal paper [23], the MLP-Mixer is, at its core, a convolutional neural network with very specific architectural hyper-parameters. As such, the MLP-Mixer can exploit the existing GPU architectures and implementations that allow convolution operations to be performed with extreme efficiency, whereas attention-based networks

are currently throttled by the speed at which GPUs can perform the un-optimized attention operation.

Furthermore, the MLP-Mixer and transformer blocks differ in their usage of memory. Both the MLP-mixer block and transformer block contain a channel-mixing MLP, but the transformer uses a self-attention module in lieu of the MLP-mixer’s token-mixing MLP. Since both the transformer and MLP-mixer contain a channel-mixing MLP, we will focus on the transformer’s self-attention operator and the mixer’s token-mixing MLP for comparison.

For a representation with  $n$  tokens and  $c$  channels, the self-attention operator of the transformer block has  $\mathcal{O}(c^2)$  parameters while the token-mixing MLP of the mixer block has  $\mathcal{O}(n^2)$  parameters (Table 2). However, the main memory sink of the self-attention block comes in the intermediate activations necessary for both forward and back-propagation. For a batch size  $b$ , the  $h$ -headed self-attention module uses  $\mathcal{O}(hbn^2 + bnc)$  intermediate activation floats while the token-mixing MLP uses  $\mathcal{O}(bnc)$ . This extensive increase in activation memory comes from the token-mixing part of the attention mechanism. A separate  $n \times n$  attention score matrix is calculated for each attention head *per sample*. Thus, the memory usage term that is quadratic in  $n$  scales linearly with both  $b$  and  $h$ . It is this additional  $hbn^2$  term in the memory usage of the self-attention module that makes transformer models prohibitive for domains with a large number of tokens, such as visual data. Table 1 illustrates how quickly the memory usage of self-attention explodes with the number of tokens.

A vanilla residual block consisting of two convolutional layers with kernels of size  $k \times k$  would only have  $\mathcal{O}(k^2c^2)$  parameters and use  $\mathcal{O}(bnc)$  intermediate activation floats. Clearly, a vanilla residual block has the least memory usage and parameter count, but it lacks the capacity to account for long-range relationships between tokens as described above due to the small receptive field.

## 4. Experiments

We test MixerGAN on several datasets for unpaired image-to-image translation and include both quantitative and qualitative analysis of the results.

**Training Details** To ensure a fair comparison of the effectiveness of our MLP-based model with respect to a CNN-based model, we follow the settings of CycleGAN [28] as closely as possible. We leave downsampling and up-sampling layers as the original model but change the core translation ResNet blocks of CycleGAN to our MLP-mixer blocks. That is, we have a total of 9 MLP-Mixer blocks, as explained in section 3.2. We use the original patch discriminator in CycleGAN. We use Adam optimizer with learning rate of 0.0003, keeping the same learning rate for the first 100 epochs and linearly decaying the learning rate to



Figure 3: High-resolution results on translating between apples and oranges. Sources selected from those that gave “Best Result” on CycleGAN [28] according to the authors. Despite the patch down and up-projection, MixerGAN is still able to generate coherent, high-resolution output.

zero until the last iteration. All experiments are trained on an RTX A6000 GPU for 20,000 iterations with batch size of 16, patch size of 8x8, latent channel width of 256, and image input size of 256x256 pixels (unless otherwise specified).

**Baselines** We compare our results with CNN-based CycleGAN [28], DiscoGAN [10], DualGAN [27], UNIT [12] and with attention-based models from Mejjati et al. [1], SPA-GAN [4], and Residual Attention (RA) [25]. To ensure a fair comparison, we reproduce CycleGAN, and evaluate our method on Kernel Inception Distance (KID) [2]

scores. While Frèchet Inception Distance (FID) is a more commonly used metric today, many of the models to which we are comparing only report KID. We unfortunately do not have the compute to reproduce all these other models in a reasonable amount of time to determine their FIDs, so we only report our comparisons in terms of KID. Since this is an exploratory work to show the feasibility of MLP-based image-to-image translation and not a claim of state-of-the-art performance, we maintain that the KID comparison is sufficient.

Algorithm	KID ( $\downarrow$ )			
	A $\rightarrow$ O	O $\rightarrow$ A	H $\rightarrow$ Z	Z $\rightarrow$ H
DiscoGAN [10]	18.34 $\pm$ 0.75	21.56 $\pm$ 0.80	13.68 $\pm$ 0.28	16.60 $\pm$ 0.50
RA [25]	12.75 $\pm$ 0.49	13.84 $\pm$ 0.78	10.16 $\pm$ 0.12	10.97 $\pm$ 0.26
DualGAN [27]	13.04 $\pm$ 0.72	12.42 $\pm$ 0.88	10.38 $\pm$ 0.31	12.86 $\pm$ 0.50
UNIT [12]	11.68 $\pm$ 0.43	11.76 $\pm$ 0.51	11.22 $\pm$ 0.24	13.63 $\pm$ 0.34
CycleGAN [28]	8.48 $\pm$ 0.53	9.82 $\pm$ 0.51	10.25 $\pm$ 0.25	11.44 $\pm$ 0.38
CycleGAN (reproduced)	8.42 $\pm$ 0.49	13.71 $\pm$ 0.62	3.53 $\pm$ 0.9	4.91 $\pm$ 0.67
UA [1]	6.44 $\pm$ 0.69	5.32 $\pm$ 0.48	6.93 $\pm$ 0.27	8.87 $\pm$ 0.26
SPA-GAN [4]	3.77 $\pm$ 0.32	2.38 $\pm$ 0.33	2.01 $\pm$ 0.13	2.19 $\pm$ 0.12
MixerGAN (Ours)	10.23 $\pm$ 0.69	4.50 $\pm$ 0.44	6.81 $\pm$ 0.12	13.99 $\pm$ 0.25

Table 3: Kernel Inception Distance  $\times 100 \pm$  std.  $\times 100$  for different image translation algorithms. Lower is better. Abbreviations: A - Apple, O - Orange, H - Horse, Z - Zebra.

**Datasets** We use the following datasets for image-to-image translation provided by Zhu et al. [28]: Apple-to-Orange (A  $\leftrightarrow$  O), containing 995/266 train/test apple images and 1019/248 train/test orange images; Horse-to-Zebra (H  $\leftrightarrow$  Z), containing 1067/120 train/test horse images and 1334/140 train/test zebra images; and Yosemite Summer-to-Winter (S  $\leftrightarrow$  W), containing 1231/309 train/test summer images, and 962/238 train/test winter images.

## 5. Results

As previously stated, the objective of this work is not to achieve state-of-the-art results or out-perform any baselines. Instead, our purpose is to show that an MLP-based architecture can effectively perform image-to-image translation while accounting for long-range connections not possible with convolution and being much less computationally expensive than a transformer-based model. Adapting further improvements upon the CycleGAN architecture to MixerGAN, such as contrastive learning [18], are left as the subject of future work.

### 5.1. Quantitative Results

For completion’s sake, we include a quantitative comparison of MixerGAN’s with other popular image-to-image translation algorithms.

To quantitatively evaluate our model, we use Kernel Inception Distance (KID) [2]. KID computes the squared maximum mean discrepancy between real and fake images using feature representations, extracted from the Inception network architecture [21]. Similar to Fréchet Inception Distance (FID) metric [7], and even though KID is not bounded, a lower score implies the generated distribution is closer to the real distribution such that it is visually more similar. We compute KID scores on unidirectional mappings, from  $X$  to  $Y$  and vice-versa.

On all tasks, MixerGAN performs within the same KID

range as the other models, as seen in Table 3. Compared directly to CycleGAN [28], MixerGAN significantly outperforms both the authors’ originally reported and our reproduced KID values on the Orange-to-Apple task while remaining in the same ballpark for tasks on which it scored worse. Recall, our goal is **not** to outperform current methods, but to instead show the feasibility of MLP-based models as a vehicle for image-to-image translation. The fact that MixerGAN scores quantitatively in the same range as current models supports this idea.

### 5.2. Qualitative Results

For our qualitative results, we compare the output of our model to that of CycleGAN [28] on images that the CycleGAN authors note gave them the best results.

**Comparing Apples and Oranges** In Figure 3, we present our results in large resolution so the reader can appreciate that our MixerGAN can produce images of the same fidelity as CycleGAN. For the sake of space, we do not repeat this for our other datasets. Examining Figure 3, we see that not only can MixerGAN create images of similar quality as CycleGAN, but it even improves upon it in some cases. In the first row, we see that CycleGAN generated an unrealistic combination of the inside and outside of an orange while MixerGAN generated a coherent-looking orange. In the third row, we see that CycleGAN retained the orange’s texture in the generated apple, especially near the specular reflections. In contrast, MixerGAN correctly synthesizes the typical apple texture, including around the specular reflections.

**Yosemite Dataset** Our model sees an encouraging level of success on the Yosemite dataset. In Figure 4, we see the results of MixerGAN compared to those of CycleGAN

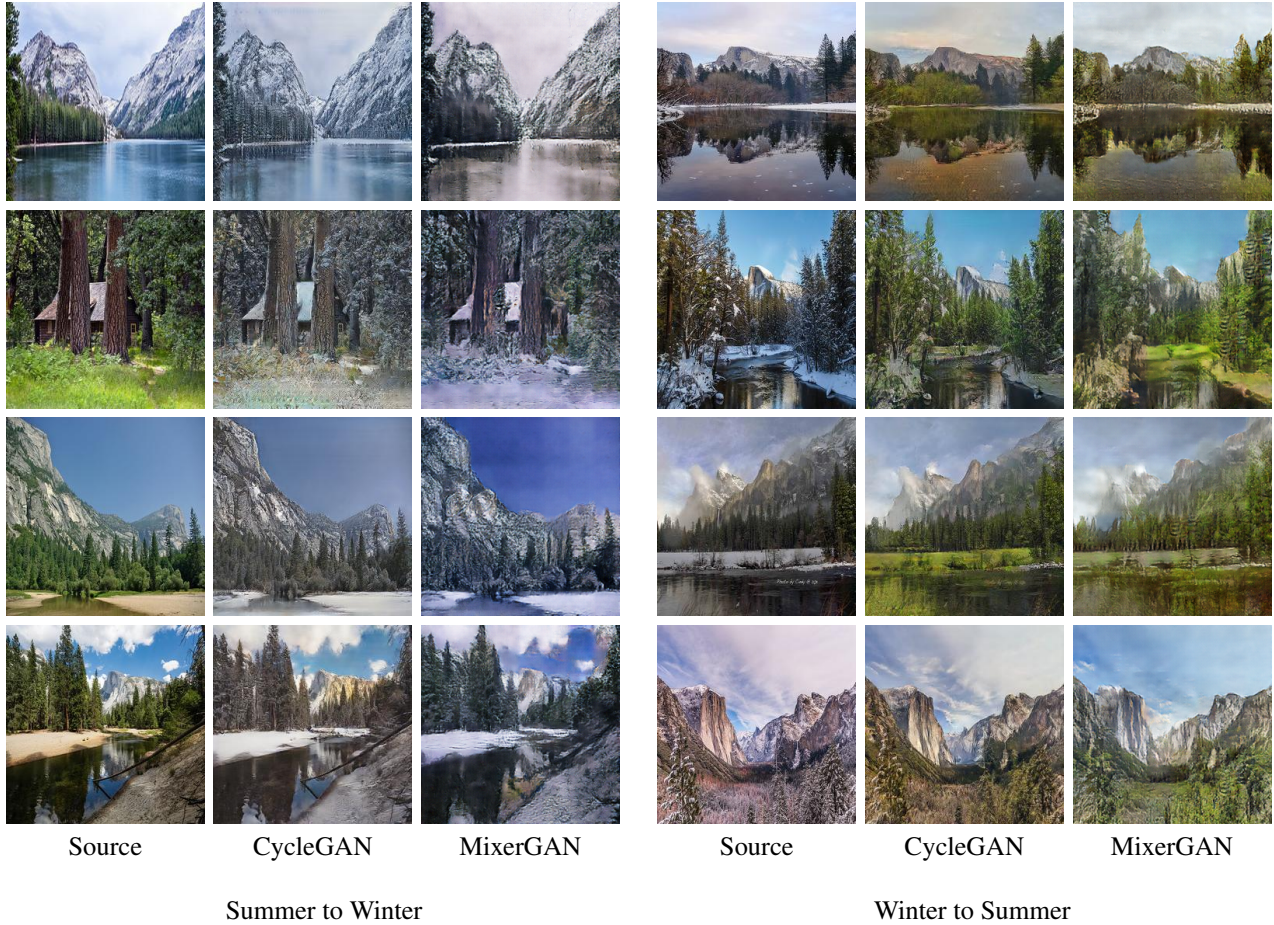


Figure 4: Results on the Yosemite dataset. MixerGAN better captures the vibrant whites and purples of winter and blues and greens of summer while CycleGAN has a more muted pallet.

[28] on some of the “best” images as selected by the CycleGAN authors. From a purely subjective standpoint, MixerGAN seems to do a better job achieving the vibrant colors of the respective seasons. Specifically, we see in the synthetic winter images that MixerGAN generates much whiter snow and more purple skies whereas CycleGAN tends to generate a blue-gray haze. In the synthetic summer images, MixerGAN generates significantly more saturated blues and greens while CycleGAN yields a more muted palette.

**Horses to Zebras** The Horse to Zebra dataset posed a large challenge for our model. When run on 256x256 images, the results were full of patch artifacts. We hypothesize that this is due to the previously mentioned information loss at the patch projection step and could be placated by using more channels in the latent representation. We then tried our model on 128x128 images and reached much better re-

sults for Horse to Zebra as seen in Figure 5 but still not for Zebra to Horse.

### 5.3. Failure Modes and Limitations

The largest limiting factor of the MixerGAN model seems to come from the patch projection step. If our patch size is  $(p \times p)$ , then the spatial resolution is effectively reduced by a factor of  $p^2$ . If we only multiply the number of channels by 2 at the projection step, then we only retain  $2/p^2$  of our activation dimensionality. In our experiments, we used a patch size of  $(8 \times 8)$ , so depending on the rank of our data at that point in the network and its effective compressibility, we could potentially lose almost 97% of our information through the patch projection. Given that neighboring pixels are typically highly correlated, the practical information loss is likely much less, but it still limits the translating capacity of our generator.

Given the limitations of the patch projection step, we

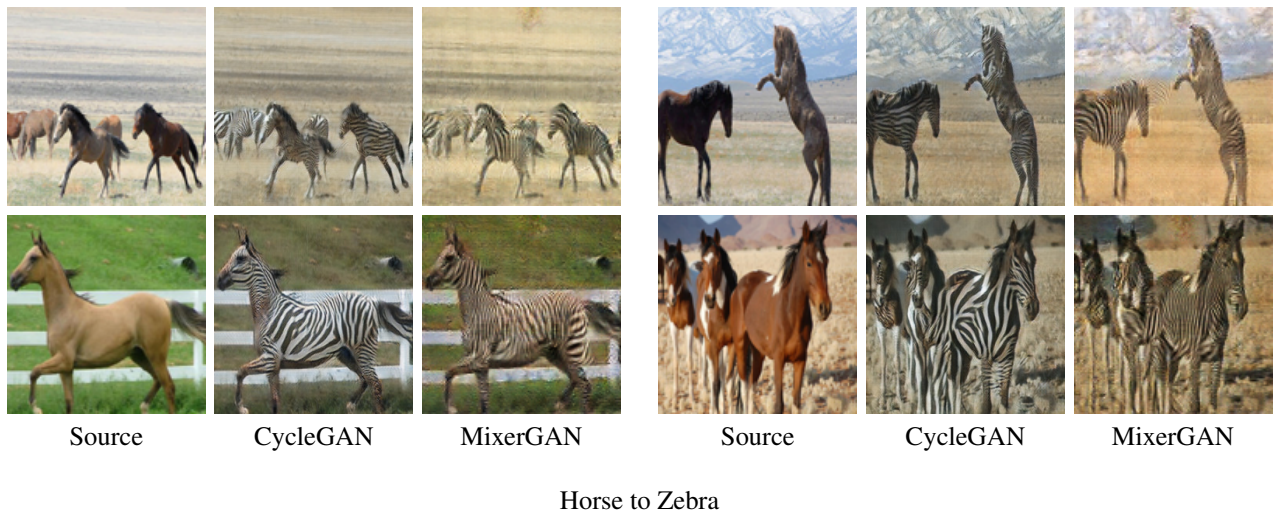


Figure 5: By using a target resolution of 128x128 instead of 256x256, we were able to obtain high-fidelity Horse to Zebra translations. However, the Zebra to Horse translations (not pictured) were still low quality.

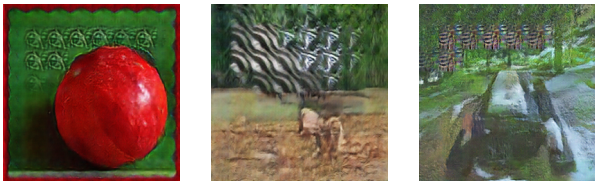


Figure 6: MixerGAN’s most common failure mode is the repetition of an identical patch artifact. We hypothesize this would be less severe in a MixerGAN with a larger number of latent channels such that less information is destroyed at the patch projection step.

sometimes find “patch” artifacts in our generated images as seen in Figure 6. We hypothesize that a larger number of channels after our patch projection step would help alleviate this artifacting issue by stymieing the information loss at that point. A less under-complete representation at the translating phase would ideally result in less compression and a more expressive model overall. Unfortunately, with our modest amount of computing power, we were not able to experiment with wider networks at this time.

## 6. Conclusions

The recent proposal of the MLP-Mixer model for vision showed that multi-layer perceptrons can still be effective for visual classification tasks in the modern age of deep learning. In this work, we have shown that the MLP-Mixer is also an effective architecture for generative models, specifically unpaired image-to-image translation. We hypothesize

that increasing the number of channels in the latent space would reduce any patch artifacting and hope to obtain computing resources to investigate this in the future.

Like all image synthesis applications, MixerGAN has the potential to be used for potentially malicious goals, such as deepfakes [17]. As such, synthetic image detection continues to be an important field of its own. However, this should not deter us from continuing research in image synthesis, as the best way to combat a threat is to thoroughly understand it.

After decades of convolutional neural networks (and more recently, transformer networks) dominating the field of computer vision, it is remarkable that a simple sequence of weight-tied MLPs can effectively perform the same tasks. Now that we have shown that the MLP-Mixer succeeds at generative objectives, the door is open to refine this technique and extend MLP-based architectures to further image synthesis tasks.

## References

- [1] Youssef Alami Mejjati, Christian Richardt, James Tompkin, Darren Cosker, and Kwang In Kim. Unsupervised attention-guided image-to-image translation. In S. Bengio, H. Wallach, H. Larochelle, K. Grauman, N. Cesa-Bianchi, and R. Garnett, editors, *Advances in Neural Information Processing Systems*, volume 31. Curran Associates, Inc., 2018.
- [2] Mikołaj Bińkowski, Dougal J Sutherland, Michael Arbel, and Arthur Gretton. Demystifying mmd gans. *arXiv preprint arXiv:1801.01401*, 2018.
- [3] Yun Cao, Zhiming Zhou, Weinan Zhang, and Yong Yu. Unsupervised diverse colorization via generative adversarial



- networks. In *Joint European conference on machine learning and knowledge discovery in databases*, pages 151–166. Springer, 2017.
- [4] Hajar Emami, Majid Moradi Aliabadi, Ming Dong, and Ratna Babu Chinnam. Spa-gan: Spatial attention gan for image-to-image translation. *IEEE Transactions on Multimedia*, 23:391–401, 2020.
- [5] Ian J Goodfellow, Jean Pouget-Abadie, Mehdi Mirza, Bing Xu, David Warde-Farley, Sherjil Ozair, Aaron Courville, and Yoshua Bengio. Generative adversarial networks. *arXiv preprint arXiv:1406.2661*, 2014.
- [6] Dan Hendrycks and Kevin Gimpel. Gaussian error linear units (gelus). *arXiv preprint arXiv:1606.08415*, 2016.
- [7] Martin Heusel, Hubert Ramsauer, Thomas Unterthiner, Bernhard Nessler, and Sepp Hochreiter. Gans trained by a two time-scale update rule converge to a local nash equilibrium. *arXiv preprint arXiv:1706.08500*, 2017.
- [8] Xun Huang, Ming-Yu Liu, Serge Belongie, and Jan Kautz. Multimodal unsupervised image-to-image translation. In *Proceedings of the European conference on computer vision (ECCV)*, pages 172–189, 2018.
- [9] Phillip Isola, Jun-Yan Zhu, Tinghui Zhou, and Alexei A Efros. Image-to-image translation with conditional adversarial networks. In *Proceedings of the IEEE conference on computer vision and pattern recognition*, pages 1125–1134, 2017.
- [10] Taeksoo Kim, Moonsu Cha, Hyunsoo Kim, Jung Kwon Lee, and Jiwon Kim. Learning to discover cross-domain relations with generative adversarial networks. In *International Conference on Machine Learning*, pages 1857–1865. PMLR, 2017.
- [11] Christian Ledig, Lucas Theis, Ferenc Huszár, Jose Caballero, Andrew Cunningham, Alejandro Acosta, Andrew Aitken, Alykhan Tejani, Johannes Totz, Zehan Wang, et al. Photo-realistic single image super-resolution using a generative adversarial network. In *Proceedings of the IEEE conference on computer vision and pattern recognition*, pages 4681–4690, 2017.
- [12] Ming-Yu Liu, Thomas Breuel, and Jan Kautz. Unsupervised image-to-image translation networks. *arXiv preprint arXiv:1703.00848*, 2017.
- [13] Ming-Yu Liu and Oncel Tuzel. Coupled generative adversarial networks. *arXiv preprint arXiv:1606.07536*, 2016.
- [14] Xudong Mao, Qing Li, Haoran Xie, Raymond YK Lau, Zhen Wang, and Stephen Paul Smolley. Least squares generative adversarial networks. In *Proceedings of the IEEE international conference on computer vision*, pages 2794–2802, 2017.
- [15] Giovanni Mariani, Florian Scheidegger, Roxana Istrate, Costas Bekas, and Cristiano Malossi. Bagan: Data augmentation with balancing gan. *arXiv preprint arXiv:1803.09655*, 2018.
- [16] Zak Murez, Soheil Kolouri, David Kriegman, Ravi Ramamoorthi, and Kyungnam Kim. Image to image translation for domain adaptation. In *Proceedings of the IEEE Conference on Computer Vision and Pattern Recognition*, pages 4500–4509, 2018.
- [17] Thanh Thi Nguyen, Quoc Viet Hung Nguyen, Cuong M. Nguyen, Dung Nguyen, Duc Thanh Nguyen, and Saeid Nahavandi. Deep learning for deepfakes creation and detection: A survey, 2021.
- [18] Taesung Park, Alexei A Efros, Richard Zhang, and Jun-Yan Zhu. Contrastive learning for unpaired image-to-image translation. In *European Conference on Computer Vision*, pages 319–345. Springer, 2020.
- [19] Adam Paszke, Sam Gross, Francisco Massa, Adam Lerer, James Bradbury, Gregory Chanan, Trevor Killeen, Zeming Lin, Natalia Gimelshein, Luca Antiga, Alban Desmaison, Andreas Kopf, Edward Yang, Zachary DeVito, Martin Raison, Alykhan Tejani, Sasank Chilamkurthy, Benoit Steiner, Lu Fang, Junjie Bai, and Soumith Chintala. Pytorch: An imperative style, high-performance deep learning library. In H. Wallach, H. Larochelle, A. Beygelzimer, F. d’Alché-Buc, E. Fox, and R. Garnett, editors, *Advances in Neural Information Processing Systems 32*, pages 8024–8035. Curran Associates, Inc., 2019.
- [20] Matthew E Peters, Mark Neumann, Mohit Iyyer, Matt Gardner, Christopher Clark, Kenton Lee, and Luke Zettlemoyer. Deep contextualized word representations. *arXiv preprint arXiv:1802.05365*, 2018.
- [21] Christian Szegedy, Vincent Vanhoucke, Sergey Ioffe, Jon Shlens, and Zbigniew Wojna. Rethinking the inception architecture for computer vision. In *Proceedings of the IEEE conference on computer vision and pattern recognition*, pages 2818–2826, 2016.
- [22] Hao Tang, Hong Liu, Dan Xu, Philip HS Torr, and Nicu Sebe. Attentiongan: Unpaired image-to-image translation using attention-guided generative adversarial networks. *arXiv preprint arXiv:1911.11897*, 2019.
- [23] Ilya Tolstikhin, Neil Houlsby, Alexander Kolesnikov, Lucas Beyer, Xiaohua Zhai, Thomas Unterthiner, Jessica Yung, Daniel Keysers, Jakob Uszkoreit, Mario Lucic, et al. Mlp-mixer: An all-mlp architecture for vision. *arXiv preprint arXiv:2105.01601*, 2021.
- [24] Ashish Vaswani, Noam Shazeer, Niki Parmar, Jakob Uszkoreit, Llion Jones, Aidan N Gomez, Lukasz Kaiser, and Illia Polosukhin. Attention is all you need. In *NIPS*, 2017.
- [25] Fei Wang, Mengqing Jiang, Chen Qian, Shuo Yang, Cheng Li, Honggang Zhang, Xiaogang Wang, and Xiaoou Tang. Residual attention network for image classification. In *Proceedings of the IEEE conference on computer vision and pattern recognition*, pages 3156–3164, 2017.
- [26] Bingzhe Wu, Haodong Duan, Zhichao Liu, and Guangyu Sun. Srpgan: perceptual generative adversarial network for single image super resolution. *arXiv preprint arXiv:1712.05927*, 2017.
- [27] Zili Yi, Hao Zhang, Ping Tan, and Minglun Gong. Dualgan: Unsupervised dual learning for image-to-image translation. In *Proceedings of the IEEE international conference on computer vision*, pages 2849–2857, 2017.
- [28] Jun-Yan Zhu, Taesung Park, Phillip Isola, and Alexei A Efros. Unpaired image-to-image translation using cycle-consistent adversarial networks. In *Proceedings of the IEEE international conference on computer vision*, pages 2223–2232, 2017.

## A. Mixer Block and Generator Code

```
class CycleGeneratorMixer(nn.Module):

    def __init__(self, patch_dim, image_size=256, embed_dim=256, transform_layers=9,
                 patch_size=8):
        super(CycleGeneratorMixer, self).__init__()

        # stem
        model = [
            nn.Conv2d(in_channels=3, out_channels=embed_dim//4, kernel_size=7,
                      padding=3, padding_mode='reflect'),
            nn.InstanceNorm2d(embed_dim//4),
            nn.ReLU(True),
            # PrintLayer(name='stem')
        ]

        # downsampling
        model += [
            nn.Conv2d(in_channels=embed_dim//4, out_channels=embed_dim//2,
                      kernel_size=3, stride=2, padding=1),
            nn.InstanceNorm2d(embed_dim//2),
            nn.ReLU(True),
            nn.Conv2d(in_channels=embed_dim//2, out_channels=embed_dim, kernel_size=3,
                      stride=2, padding=1),
            nn.InstanceNorm2d(embed_dim),
            nn.ReLU(True),
        ]

        # linear down-projection
        model += [nn.Conv2d(in_channels=embed_dim, out_channels=embed_dim,
                             kernel_size=patch_size, stride=patch_size)]

        # reshape to (tokens, channels)
        model += [View((embed_dim, patch_dim))]

        # transformation
        model += [MixerBlock(embed_dim=embed_dim, patch_dim=patch_dim)
                  for _ in range(transform_layers)]

        # reshape to (c, h, w)
        model += [View((embed_dim, image_size//4//patch_size,
                       image_size//4//patch_size))]

        # linear up-projection
        model += [nn.ConvTranspose2d(in_channels=embed_dim, out_channels=embed_dim,
                                     kernel_size=patch_size, stride=patch_size)]

        # upsampling
        model += [
            nn.ConvTranspose2d(in_channels=embed_dim, out_channels=embed_dim//2,
                              kernel_size=3, stride=2, padding=1, output_padding=1),
            nn.InstanceNorm2d(embed_dim//2),
            nn.ReLU(True),
```

```

        nn.ConvTranspose2d(in_channels=embed_dim//2, out_channels=embed_dim//4,
                           kernel_size=3, stride=2, padding=1, output_padding=1),
        nn.InstanceNorm2d(embed_dim//4),
        nn.ReLU(True),
    ]

```

```

# to RGB
model += [nn.Conv2d(in_channels=embed_dim//4, out_channels=3, kernel_size=7,
                    padding=3, padding_mode='reflect')]

```

```

model += [nn.Tanh()]

```

```

self.model = nn.Sequential(*model)

```

```

def forward(self, x):
    return self.model(x)

```

```

class MixerBlock(nn.Module):
    def __init__(self, embed_dim, patch_dim):
        super(MixerBlock, self).__init__()
        self.ln1 = nn.LayerNorm([embed_dim, patch_dim])

        self.dense1 = nn.Linear(in_features=patch_dim, out_features=patch_dim,
                                bias=False)

        self.gelu1 = nn.GELU()
        self.dense2 = nn.Linear(in_features=patch_dim, out_features=patch_dim,
                                bias=False)

        self.ln2 = nn.LayerNorm([embed_dim, patch_dim])

        # using conv1d with kernel_size=1 is like applying a
        # linear layer to the channel dim
        self.conv1 = nn.Conv1d(in_channels=embed_dim, out_channels=embed_dim,
                                kernel_size=1, bias=False)

        self.gelu2 = nn.GELU()
        self.conv2 = nn.Conv1d(in_channels=embed_dim, out_channels=embed_dim,
                                kernel_size=1, bias=False)

    def forward(self, x):
        # token-mixing mlp
        skip = x
        x = self.ln1(x)
        x = self.dense1(x)
        x = self.gelu1(x)
        x = self.dense2(x)
        x = x + skip

```

```
# channel-mixing mlp
skip = x
x = self.ln2(x)
x = self.conv1(x)
x = self.gelu2(x)
x = self.conv2(x)
x = x + skip

return x
```